Journal of Membrane Science 551 (2018) 305–314

Contents lists available at ScienceDirect

Journal of Membrane Science

journal homepage: www.elsevier.com/locate/memsci

Triptycene-containing poly(benzoxazole-*co*-imide) membranes with enhanced mechanical strength for high-performance gas separation

Shuangjiang Luo[a], Qinnan Zhang[a], Tyler K. Bear[a], Tyler E. Curtis[b], Ryan K. Roeder[b], Cara M. Doherty[c], Anita J. Hill[c], Ruilan Guo[a,*]

[a] Department of Chemical and Biomolecular Engineering, University of Notre Dame, Notre Dame, IN 46556, USA
[b] Department of Aerospace and Mechanical Engineering, University of Notre Dame, Notre Dame, IN 46556, USA
[c] The Commonwealth Scientific and Industrial Research Organization (CSIRO) Manufacturing, Private Bag 10, Clayton, South Victoria 3169, Australia

ARTICLE INFO

Keywords:
Poly(benzoxazole-*co*-imide)
Triptycene
Thermal rearrangement (TR)
Mechanical properties
Gas separation membrane

ABSTRACT

Herein, a series of novel triptycene-containing thermally rearranged poly(benzoxazole-*co*-imide) membranes (TPI-PBOs) with enhanced mechanical properties and gas separation performance are reported. The effects of chemical structures and poly(benzoxazole-*co*-imide) composition on the fractional free volume, polymer chain packing, microcavity size and size distribution, mechanical properties, and gas transport properties have been comprehensively investigated. Due to the incorporation of triptycene-containing non-TR-able polyimide segments, the resulting poly(benzoxazole-*co*-imide) films exhibited good mechanical properties even after being treated at 450 °C. The incorporation of bulky and rigid triptycene units led to significantly improved fractional free volume and gas transport properties compared to previously reported poly(benzoxazole-*co*-imide)s. Several triptycene-containing poly(benzoxazole-*co*-imide) films displayed excellent gas separation performance for H_2/CH_4, H_2/N_2, and CO_2/CH_4 gas pairs that exceeded the 2008 upper bounds.

1. Introduction

Polymeric gas separation membranes have attracted great interests and been used in natural gas sweetening, air separation, hydrogen purification as well as carbon capture during the past decades due to their advantages of low energy consumption, small footprint, and flexibility of operation and low maintenance [1–3]. In particular, mechanical robust membrane materials with a combination of high permeability and high selectivity are demanded for practical applications to reduce membrane area and increase product purity. Recent research efforts have been focused on the fabrication of highly microporous materials with high fractional free volume (FFV), such as polymers of intrinsic microporosity (PIM) featuring ladder-like structures with kinked sites [4–6], Tröger's base polymers consisting of benzene rings fused by rigid bridged bicyclic units [7,8], and thermally rearranged (TR) polymers with stiff polybenzoxazole (PBO) main chain structures [9]. Due to the high microporosity generated by the rigid and contorted backbone structures in these polymers, they demonstrate ultrahigh gas permeabilities and good gas selectivities, many of which have exhibited separation performance well beyond the Robeson's upper bounds [10,11]. Compared to PIMs and Tröger's base polymers that typically involve rather complicated monomer synthesis and polymerization, TR polymers with PBO structure can be relatively facilely prepared via solid-state thermal treatment of poly(hydroxyimide) precursors [9,12–16] or poly(hydroxyamide) precursors [17–20], both of which involve simply conventional polycondensation reaction between diamines and dianhydrides or diacid chlorides. During thermal conversion of imide or amide structures to rigid coplanar benzoxazole structure, the significant configurational and conformational changes result in high FFV and microporosity, enabling extraordinary gas separation performance in corresponding TR-PBO polymers [9]. However, mechanical properties of TR polymers are typically compromised during thermal treatment possibly due to the thermal decomposition occurring at high temperatures (> 400 °C), which hinders their practical implementation.

Recently, several strategies have been applied to address the issue of insufficient mechanical properties of TR polymers. For instance, the incorporation of spirobisindane units improved both tensile strength (69.9–94.4 MPa) and ductility (elongation at break of 15 − 20%) of TR polymers due to enhanced chain entanglement and reduced elongational stress [21]. Introducing flexible ether linkages was shown to lower the thermal rearrangement temperature, which reduce the probability of thermal degradation during thermal treatment, resulting in improved elongation at break [22]. Preparing TR copolymers based

* Corresponding author.
E-mail address: rguo@nd.edu (R. Guo).

https://doi.org/10.1016/j.memsci.2018.01.052
Received 4 December 2017; Received in revised form 16 January 2018; Accepted 22 January 2018
Available online 31 January 2018
0376-7388/

on poly(benzoxazole-*co*-imide) structure (PBO-*co*-PI) appeared to be an effective approach to enhance the mechanical properties of TR membranes [12,23–25]. For example, the tensile strength and elongation at break reached up to 113.9 MPa and 13.4%, respectively, for a TR-PBOI copolymer thermally treated at 400 °C for 1 h [12]. However, due to the presence of non-TR-able polyimide segments, poly(benzoxazole-*co*-imide) copolymers always showed inferior gas separation performance compared to TR homopolymers. In this regard, new poly(benzoxazole-*co*-imide) precursor structures are needed to achieve simultaneously both high mechanical strength and excellent gas transport properties.

Incorporating iptycene structures (e.g., triptycene and pentiptycene) into microporous polymers such as polyimides [26–33], PIMs [5,6,8], TR polymers [34–36], has attracted much attention recently for gas separation membranes. The bulkiness and rigid frameworks of iptycene units can induce significant disruption of chain packing and result in high microporosity and fractional free volume for high permeability. Moreover, the internal free volume microcavities in between the benzene "blades" of iptycene moieties uniquely provide excellent size sieving properties because the size of these permanent molecular cavities are similar to the kinetic diameters of common penetrant gas molecules of interest (e.g., He, H_2, CO_2, O_2, N_2, CH_4, C_2H_4, C_3H_6). As such, iptycene approach provides a completely new platform to finely tune the microcavity size for permeation of smaller gases and exclusion of larger gases. Previous studies have demonstrated that incorporation of triptycene units into TR polymers creates high microporosity and ultrafine-microporosity, enabling both high gas permeabilities and high selectivities for a variety of gas pairs [35,36].

Based on the abovementioned considerations, we sought in this study an integration of poly(benzoxazole-*co*-imide) and iptycene structures to address the issues of inferior gas transport properties of previous TR copolymers and deteriorated mechanical properties of TR homopolymers. In particular, triptycene units are introduced into the non-TR-able polyimide units to produce a series of triptycene-containing poly(imide-co-hydroxyimide) copolymer precursors, i.e., TPI-PHI. Specifically, condensation copolymerizations are carried out from commercial 4,4′-hexafluoroisopropylidene bisphthalic dianhydride (6FDA), 2,2′-bis(3-amino-4-hydroxyphenyl)hexafluoropropane (6FAP), and custom-synthesized triptycene-1,4-diamine monomer in varying feeding ratios. Correspondingly, a set of novel triptycene-containing poly(benzoxazole-*co*-imide)s (TPI-PBO) with varying PBO content are prepared by the solid-state TR process of TPI-PHI copolymer precursors (Scheme 1). Physical properties including FFV, inter-chain packing, microcavity size and pore size distribution, and mechanical properties, and gas transport properties have been systematically examined and reported. Comparisons between the new triptycene-containing TPI-PBOs and previously reported non-triptycene poly(benzoxazole-*co*-imide) copolymers show triptycene's enhancement in both gas separation performance and mechanical robustness.

2. Experimental

2.1. Materials

Triptycene-1,4-diamine (TPDAm) was prepared according to previous reports [37,38], and was recrystallized in ethanol and dried at 100 °C under vacuum overnight prior to use. 6FAP (> 98.5%) and 6FDA (> 99.0%) were obtained from Akron Polymer Systems (Ohio, USA) and dried at 65 and 160 °C, respectively, under vacuum before use. Anhydrous 1-methyl-2-pyrrolidinone (NMP, 99.5%, Sigma-Aldrich, USA) and 1, 2-dichlorobenzene (*o*-DCB, 99.0%, Sigma-Aldrich, USA) were used as received.

2.2. Synthesis of TPI-PHI copolyimide precursor

The triptycene-containing copolyimide precursors based on TPDAm, 6FDA and 6FAP with varying ratios of TR-able 6FDA-6FAP unit and non-TR-able 6FDA-TPDAm unit were prepared via a two-step azeotropic solution imidization process, as shown in Scheme 2. The molar amount of the non-TR-able TPDAm-6FDA unit was controlled by the molar ratio of TPDAm and 6FAP. Based on the mole fraction of triptycene-containing repeat unit (x), the obtained poly(imide-co-hydroxyimide) copolymers were named as TPI-PHI-x (x = 0.25, 0.5, and 0.75), where TPI refers to the non-TR-able TPDAm-6FDA units and PHI refers to the TR-able 6FAP-6FDA units. Taking the synthesis of TPI-PHI-0.25 as an example: in a flame-dried, three-neck flask equipped with a nitrogen inlet and a mechanical stirrer, TPDAm (0.3413 g, 1.2 mmol), 6FAP (1.3188 g, 3.6 mmol), and anhydrous NMP (15 mL) were added. After both diamine monomers were dissolved completely, the flask was immersed in an ice-water bath and 6FDA (2.1329 g, 4.8 mmol) was added; the reaction mixture was stirred continuously at r.t. overnight to form a viscous poly(amic acid) solution. Imidization was conducted at 190 °C for 12 h using *o*-DCB (5 mL) as an azeotropic agent to remove water from the Dean-Stark trap equipped flask. The resulting solution was precipitated in a methanol/water (1 L, v/v = 1:1) mixture and washed with deionized (DI) water and methanol. The fibrous solid was collected and dried at 180 °C under vacuum to give TPI-PHI-0.25 (3.72 g, yield 98.0%). ^{1}H NMR (500 MHz, DMSO-d_6): δ 5.97 (s, 2H), 6.94–6.98 (m, 8H), 7.06–7.08 (d, J = 7.70 Hz, 6H), 7.18–7.22 (m, 8H), 7.40 (s, 4H), 7.50 (s, 6H), 7.72–7.78 (m, 6H), 7.91–7.94 (m, 4H), 7.98–8.00 (m, 6H), 8.08–8.12 (m, 6H), 8.19–8.20 (d, J = 7.15 Hz, 2H), 8.28–8.30 (d, J = 7.45 Hz, 2H), 10.38–10.45 (m, 6H). ATR-FTIR (film, ν, cm^{-1}): ~3400 (br, –OH), 1786 (imide asym C=O str), 1718 (imide sym C=O str), 1370 (imide –C–N str). Molecular weight: M_w = 5.36 × 10^4 g mol^{-1}, PDI = 1.78.

Following the same procedure, TPI-PHI-0.5 was prepared from a TPDAm/6FAP molar ratio of 1:1 as a white fibrous solid (yield 97.3%). ^{1}H NMR (500 MHz, DMSO-d_6): δ 5.97–5.99 (m, 2H), 6.96–6.99 (m, 4H), 7.07 (s, 2H), 7.23 (s, 4H), 7.41 (s, 4H), 7.50 (s, 2H), 7.72–7.75 (d, J = 14.05 Hz, 2H), 7.91–7.94 (d, J = 13.90 Hz, 4H), 8.00 (s, 2H), 8.08–8.12

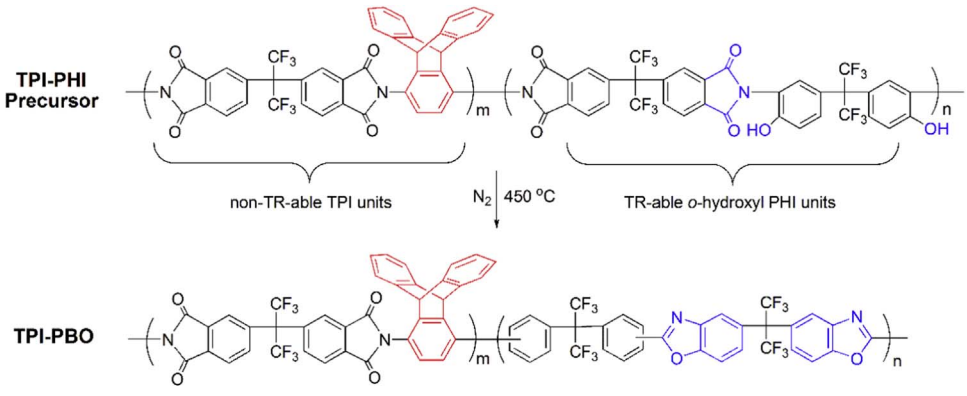

Scheme 1. Preparation of triptycene-containing poly (benzoxazole-*co*-imide), TPI-PBO, via thermal rearrangement (TR) of triptycene-containing poly (imide-*co*-hydroxyimide) precursor, TPI-PHI. m and n are adjusted by varying the molar ratio of triptycene-diamine and 6FAP.

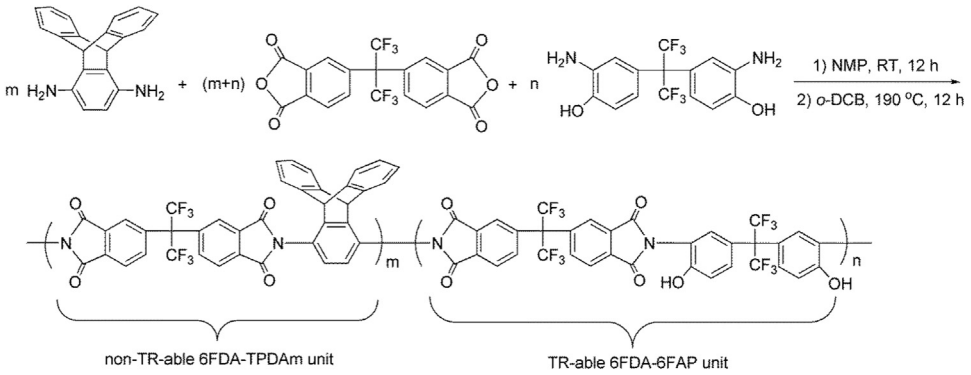

Scheme 2. Synthesis of triptycene-containing *o*-hydroxy copolyimide precursors.

(m, 2H), 8.19–8.28 (m, 2H), 8.37–8.39 (d, J = 6.50 Hz, 2H), 10.42–10.46 (m, 2H). ATR-FTIR (film, ν, cm^{-1}): ~3400 (br, –OH), 1786 (imide asym C=O str), 1721 (imide sym C=O str), 1364 (imide –C–N str). Molecular weight: $M_w = 5.65 \times 10^4$ g·mol^{-1}, PDI = 2.91.

Similarly, TPI-PHI-0.75 was obtained from a TPDAm/6FAP ratio of 3:1 as white fibrous solid with a yield of 96.8%. ^{1}H NMR (500 MHz, DMSO-d_6): δ 5.95–5.97 (m, 6H), 6.94–6.98 (m, 8H), 7.06–7.09 (m, 2H), 7.24–7.26 (m, 8H), 7.42 (s, 12H), 7.51 (s, 2H), 7.72–7.75 (m, 2H), 7.92–7.95 (m, 12H), 7.98–8.00 (m, 4H), 8.08 (s, 6H), 8.28–8.30 (m, 2H), 8.37–8.38 (d, J = 7.10 Hz, 6H), 10.42–10.45 (m, 2H). ATR-FTIR (film, ν, cm^{-1}): ~3400 (br, –OH), 1786 (imide asym C=O str), 1721 (imide sym C=O str), 1360 (imide –C–N str). Molecular weight: M_w = 4.86 × 10^4 g mol^{-1}, PDI = 1.84.

2.3. Membrane fabrication and thermal rearrangement (TR)

The *o*-hydroxy TPI-PHI copolyimide precursor films were fabricated by the solution casting method. Fibrous TPI-PHI copolyimides were dissolved in NMP to form ~8 wt% solutions, which were filtered through a 0.45 μm PTFE syringe filter and cast on flat, leveled glass plates. Solvent was evaporated slowly by placing the glass plates with polymer solutions under infrared lamps (Staco Energy Products Co., 120 V) for overnight, and the surface temperature on glass plates was around 60 °C. The resulting copolyimide films were removed from glass plates by immersion in DI water and dried in a vacuum oven at 180 °C for 24 h.

The TPI-PBO copolymer films were prepared by thermal rearrangement of the precursor TPI-PHI films under a high-purity nitrogen atmosphere. Sandwiched between two porous ceramic plates to avoid deformation during thermal treatment, the TPI-PHI precursor films were placed in a preheated Thermo-Scientific muffle furnace (model No. F47925) at 300 °C and held for 1 h to eliminate any residual solvent within the films. Then the furnace was heated up to 450 °C at a heating rate of 30 °C min^{-1}, held for 30 min to perform thermal rearrangement. Finally, the furnace was cooled down to r.t. gradually at a cooling rate of ~5 °C min^{-1}. The obtained TPI-PBO copolymers were named as TPI-PBO-x (x = 0.25, 0.5, and 0.75) according to the mole fraction of the triptycene-containing polyimide segment.

2.4. Characterization methods

Attenuated total reflection Fourier transform infrared (ATR-FTIR) spectra of the polymer films were measured on a JASCO FT-IR 6300 spectrometer.^{1}H NMR spectra of the TPI-PHI copolymers were recorded on a Bruker AVANCE III HD 500 MHz spectrometer using deuterated dimethylsulfone (DMSO-d_6) as the solvent. Molecular weight and molecular weight distribution of the copolyimide precursors were evaluated using gel permeation chromatography (GPC, Waters GPC System) with a Waters 2414 refractive index detector and three Polymer Standards Service (PSS) columns (GRAM, 10^4, 10^3, and 10^2 Å) in DMF at 55 °C on the basis of standard poly(methyl methacrylate). Glass transition temperatures (T_g) of the copolyimide precursors were measured by differential scanning calorimetry (DSC) on a TA Instruments Q2000 in nitrogen atmosphere. Two heating-cooling cycles, in which the temperature ranges were 100–300 °C and 100–400 °C, respectively, were performed with a heating rate of 10 °C min^{-1} and a cooling rate of 20 °C min^{-1}, and T_g was determined based on the second heating cycle. Thermo-gravimetric analysis (TGA) was performed on a TA Instruments Q500 with a heating rate of 10 °C min^{-1} and a nitrogen purge of 50 mL min^{-1}. TGA isothermals were also recorded in N_2 to mimic the thermal treatment process in the furnace, in which the temperature was firstly increased (50 °C min^{-1}) to 300 °C and held for 1 h, and then increased to 450 °C (30 °C min^{-1}) and held for 30 min, and finally the temperature was decreased (5 °C min^{-1}) to 150 °C.

Wide-angle X-ray diffraction (WAXD) patterns of the films were recorded in the reflection mode on a Bruker D8 Advance Davinci diffractometer with a Cu Kα (wavelength λ = 1.54 Å) radiation source. The step size and scan speed were 0.02° per step and 5 s per step, respectively, and the average d-spacing values were calculated by means of Bragg's law in the 2θ range of 5–45°.

Mechanical properties (i.e., elastic modulus, tensile strength, and percent elongation at break) of the TPI-PHI and TPI-PBO films were tested using a Bose ElectroForce 3300 universal tensile testing unit at room temperature following ASTM D882-12 [39] and the procedures reported in our previous research [35]; the average values were reported based on the measurements of at least five specimens.

Densities of both TPI-PHI and TPI-PBO films were measured in deionized (DI) water at room temperature using an analytical balance (ML204, Mettler Toledo) equipped with a density kit by the buoyancy method. Fractional free volume (FFV) was then calculated as follows:

$$FFV = \frac{V_0 - 1.3V_w}{V_0} \quad (1)$$

where V_0 is the molar volume of the polymers determined by the density measurement, and V_w is the van der Waals volume calculated from Bondi's group contribution method [40,41]. The V_w values of the copolymers were estimated via $Vw = x_1 \cdot Vw1 + x_2 \cdot Vw2$, where x_1 and x_2 are the mole fractions of TPI and PHI/PBO, respectively; V_{w1} and V_{w2} are the corresponding van der Waals volume for the two components.

The microcavity size distribution and relative intensity of free volume elements within TPI-PBO films were evaluated using positron annihilation lifetime spectroscopy (PALS) on an automated EG&G Ortec (Oak Ridge, TN) fast-fast coincidence spectrometer at room temperature. TPI-PBO films of ~ 1 × 1 cm pieces were stacked into two 2 mm thick bundles and placed on both sides of the positron source (1.5 × 10^6 Bq of ^{22}NaCl sealed in a Mylar envelope) under a vacuum of 5 × 10^{-4} Pa. The time-to-amplitude converter was extended to 200 ns for long lifetime measurements, and the coincidence unit was discharged to increase count rates. For each polymer, a minimum of five files of data with 4.5 × 10^6 integrated counts per file were collected and analyzed using either a three- or four-component fit model based on LT v9 software [42]. The first two lifetimes can be attributed to the *para-*

positronium self-annihilation (τ_1, 0.125 ns) and the free annihilation (τ_2, ~0.4 ns), respectively; the *ortho*-positronium (*o*-Ps) lifetimes (τ_3 and τ_4) were used to calculate the average sizes of microcavities within the TPI-PBO films using the Tao-Eldrup equation [43,44]:

$$\tau = \frac{1}{2}\left[1-\frac{R}{R_0}+\frac{1}{2\pi}\sin\left(\frac{2\pi R}{R_0}\right)\right] \quad (2)$$

where τ is the lifetime (ns), R is the radius of the cavity, ΔR (1.66 Å) is an empirical parameter related to the thickness of the electron layer within the pore wall. Cavity size distributions were calculated based on PAScual software [45].

Gas permeation properties of the TPI-PBO films were measured on a custom-made instrument using constant-volume/variable-pressure method at 35 °C with five ultra-high-purity (UHP) gases (H_2, CH_4, N_2, O_2, and CO_2) [46]. The permeation film samples were prepared as described previously [31] and degassed on both sides for at least 24 h before measurements. The upstream pressure was maintained at a certain pressure (i.e., 3.0, 6.4, 9.8 and 13.0 atm) and the steady-state region of pressure increment with time in downstream (volume of 42.5 cm^3) was recorded and used to calculate gas permeability coefficient as follows:

$$P = 10^{10}\frac{V_d l}{p_{up} TRA}\left[\left(\frac{dp}{dt}\right)_{ss}-\left(\frac{dp}{dt}\right)_{leak}\right] \quad (3)$$

where P (Barrer, 1 Barrer = 10^{-10} cm^3(STP) cm/cm^2 s cmHg) is the gas permeability, V_d is the downstream volume (cm^3), l is the membrane thickness (cm) which is measured using a digital micrometer, p_{up} is the upstream pressure (cmHg), T is the measurement temperature (308 K), R is the gas constant (0.278 cm^3 cmHg/cm^3(STP)·K), A is the effective film area (~0.5 cm^2) which is determined by a digital scanner (LiDE120, Canon) and ImageJ software, dp/dt is the rate of pressure increment at steady state in downstream (cmHg/s) and $(dp/dt)_{leak}$ is the leak rate of the system (cmHg/s). The ideal selectivity ($\alpha_{A/B}$) for components A and B was defined as the ratio of pure gas permeability of the two gases: $\alpha_{A/B} = P_A/P_B$. The apparent diffusivity coefficient, D, was determined from the time-lag method as $D = l^2/6\theta$, (l: film thickness; θ: lag time). Solubility coefficient was calculated via $S = P/D$ based on the solution-diffusion model.

3. Results and discussion

3.1. Synthesis of o-hydroxy copolyimide precursors (TPI-PHI)

A series of triptycene-containing copolyimides with varying *ortho*-hydroxy content were synthesized by polycondensation of TPDAm, 6FAP, and 6FDA to study the effect of composition on the microstructure and gas transport properties of the resulting TPI-PBO copolymers. Specifically, a new triptycene-based diamine monomer, i.e., triptycene-1,4-diamine (TPDAm), where two polymerizable amine groups are directly placed on the triptycene skeleton, was prepared in high total yield (~80%) and high purity. In this study, since TPDAm eliminates flexible ether linkages in our previous iptycene-based monomers [29–31,33,35,47], its corresponding copolyimides would have much more rigid backbones and consequently more permeable films are expected. Moreover, TPDAm can be synthesized via a highly efficient approach with a much higher yield when compared to other triptycene diamines such as triptycene-2,6-diamine, whose synthesis usually involves the nitration of triptycene units using strong nitric acid inevitably accompanied with side reactions and thus low yields [8,26].

The *o*-hydroxy copolyimide precursors were synthesized via in-situ solution thermal imidization. Fibrous polymers were obtained (Fig. S1a in Supporting Information) with weight-average molecular weights in the range of 48.6 − 56.5 × 10^3 g mol^{-1} (Table S1). The chemical structures of TPI-PHI copolyimides are confirmed by ^{1}H NMR and ATR-FTIR. As shown in Fig. 1, the proton signals of hydroxy groups appear at

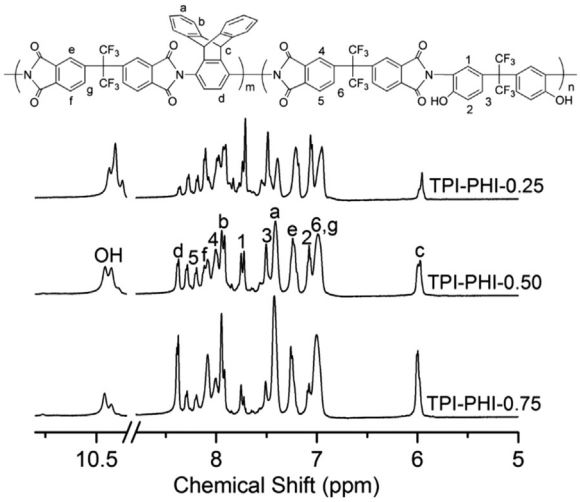

Fig. 1. ^{1}H NMR spectra of the *o*-hydroxy TPI-PHI copolyimide precursors (DMSO-d_6, 500 MHz).

10.43 ppm, and two groups of proton signals, i.e., peaks a − d and 1 − 3 are assigned to the protons of TPDAm and 6FAP moieties, respectively. The mole fractions of triptycene unit in the copolymers are determined by the peak integration ratio between the characteristic bridgehead protons of triptycene (peak c) and *o*-hydroxy protons, and the results correspond well with the target values (Table S1), revealing high reactivity of the TPDAm monomer and precise control of the copolymer compositions. In ATR-FTIR spectra (Fig. 2a), a broad peak is observed at ~3400 cm^{-1} for hydroxy groups, and the characteristic imide absorption bands are shown at around 1784 cm^{-1} (imide asymmetric carbonyl stretching), 1722 cm^{-1} (imide symmetric carbonyl stretching), and 1370 cm^{-1} (imide C − N stretching).

Previous studies have demonstrated that chain flexibility is a critical factor determining the efficiency of thermal rearrangement of *o*-hydroxy polyimide or copolyimide precursors [16,48]. Therefore, DSC was performed to determine the glass transition temperature (T_g) of the copolymers. The triptycene-containing hydroxyl copolyimides exhibit high T_g in the range of 328 − 364 °C (Table S1 and Fig. S2) suggesting high backbone rigidity as expected. On the other hand, the T_g's are much lower than the thermal treatment temperature (450 °C) used in this study which allows for sufficient local chain motion during the solid-state imide-to-benzoxazole conversion. It is also noted that the T_g of TPI-PHI copolymers increases with increasing the mole fraction of non-TR-able 6FDA-TPDAm unit. This can be ascribed to the intrinsically bulky and rigid triptycene unit structures, to which increasing fraction of imide rings are directly connected. In these copolymers, intra-chain rotational motion is greatly hindered and inter-chain triptycene-induced interactions are enhanced leading to increased overall chain rigidity. Despite the highly rigid backbone structures, the obtained copolymers are readily soluble in a variety of organic solvents, such as NMP, *N*, *N*-dimethylacetamide (DMAc), dimethylformamide (DMF), tetrahydrofuran and chloroform. Transparent thin films (Fig. S1b) were prepared by solution casting method using NMP as the casting solvent.

3.2. Thermal rearrangement of copolyimide precursors

Triptycene-containing TPI-PBO copolymers were fabricated via thermal rearrangement of the corresponding *o*-hydroxy TPI-PHI precursors (Scheme 1). TGA was performed to elucidate the solid-state thermal conversion processes as well as to establish an appropriate thermal treatment procedure. As shown in Fig. 3, all TPI-PHI precursors display two-stage weight loss TGA profiles similar to those of *o*-hydroxy homopolymers [9,14,19,20]. Specifically, the weight losses measured in the first stage under the dynamic analysis conditions (heating rate of

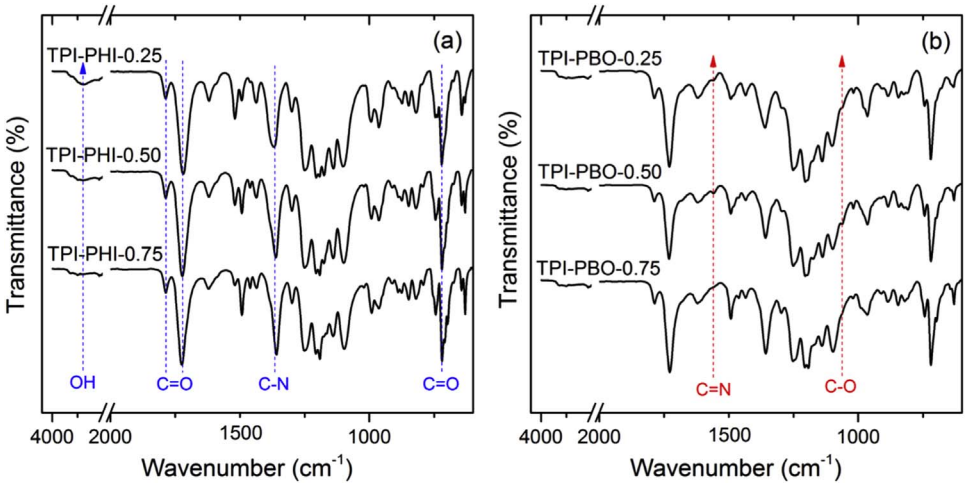

Fig. 2. ATR-FTIR spectra of (a) the *o*-hydroxy TPI-PHI copolyimide precursors and (b) thermally rearranged TPI-PBO copolymers. The arrows in the spectra indicate the decrease or increase in the intensity of specific characteristic bands.

10 °C min^{-1}) correspond fairly well with the theoretical weight loss values upon full completion of TR decarboxylation reaction (i.e., release of two CO_2 per repeat unit), confirming the occurrence of the imide-to-benzoxazole conversion. As expected, the theoretical weight loss associated with the TR conversion decreases from 8.7% to 3.1% with the increase of the non-TR-able 6FDA-TPDAm mole fraction, and the same trend was obtained in the experimental observations (Fig. 3 and Table S2). The derivatives of TGA profiles show that the peak temperatures (T_{tr}) at which weight loss reaches a maximum rate fall in the range of 411–434 °C (Table S2). This suggests a high TR temperature needs to be applied for efficient thermal conversion. The second weight loss region in TGA profiles correlates to the primary thermal decomposition of the converted poly(benzoxazole-*co*-imide) chains, and an onset degradation temperature of ~480 °C is observed for all copolymers, indicating the high thermal stability of triptycene-based polymer structures as revealed in our previous studies as well [29,33]. Based on the TGA analysis described above, the thermal treatment protocol of 450 °C for 0.5 h was chosen to promote efficient imide-to-benzoxazole conversion as well as to prevent thermal degradation during the TR process.

The imide-to-benzoxazole conversion was also evidenced by ATR-FTIR spectra showing the chemical structural changes after the thermal treatment. As shown in Fig. 2b, the broad stretching vibration peak of hydroxyl groups (~3400 cm^{-1}) of polyimide precursors disappears, and new peaks at around 1557 and 1060 cm^{-1} due to −C=N and −C−O stretching of benzoxazole units, respectively, show up after the thermal treatment at 450 °C for 0.5 h, confirming the formation of benzoxazole structure. Besides, benzoxazole absorptions decrease with increasing content of non-TR-able TPI units with TPI-PBO-0.25 displays the most intense peaks. This trend is consistent with the PBO mole fraction of the copolymers. The generally weak PBO absorbance bands can be ascribed partially to the relatively low PBO concentrations in the copolymers and the stable structure of benzoxazole rings. The low absorbance of PBO bands have been frequently observed in other PBO-based polymers [16,19,21,35,49]. The completeness of imide-to-benzoxazole conversion of the TPI-PHI copolyimide precursors is quantitatively indicated from TGA isothermal experiments by comparing experimentally observed weight losses and theoretical weight losses, and the results are shown in Table S2. All three copolymers exhibit higher experimental weight losses than the theoretical ones of TR process, suggesting complete conversion of the *o*-hydroxy copolyimide precursors. The marginal extra weight losses (1.7 − 2.1%) can be ascribed to the polymer chain degradation.

3.3. Polymer chain packing and microporosity

Fractional free volume (FFV) of both TPI-PHI copolyimide precursors and the resulting TPI-PBO copolymers were estimated using Eq. (1) to elucidate how triptycene structure and PBO composition affect microporosity and gas transport properties of the resulting TPI-PBO films. As shown in Table 1, TPI-PBO films exhibit FFV values in the range of 19.3 − 20.4%, which are expectedly higher than those of the TPI-PHI precursors (15.6 − 16.6%) due to the formation of more rigid, co-planar PBO structures [9]. TPI-PBO copolymers in this study display higher FFV than that of non-triptycene-containing poly(benzoxazole-*co*-imide)s, such as TR-PBOI series [12,24] and TR-PBO-co-I series [23], confirming that the incorporation of triptycene moieties in the poly (benzoxazole-*co*-imide) is instrumental in constructing microporous structure for fast gas transport.

For TPI-PHI precursors, an increasing FFV trend with the mole content of triptycene-containing 6FDA-TPDAm units is observed. This is

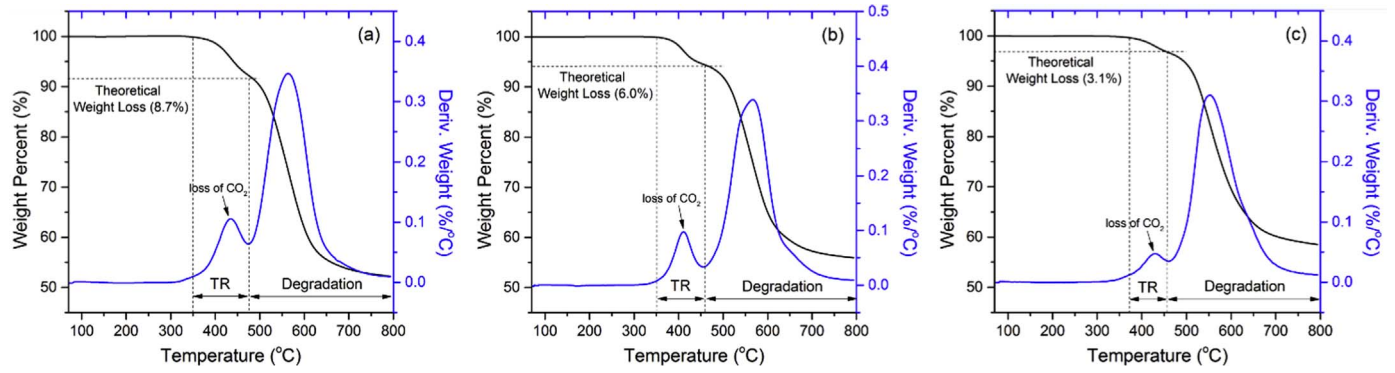

Fig. 3. Thermogravimetric analyses for (a) TPI-PHI-0.25, (b) TPI-PHI-0.50, and (c) TPI-PHI-0.75 copolyimide precursors. Theoretical weight losses during TR processes are shown by the horizontal dash lines and vertical dash lines denote regions of TR and decomposition.

Table 1
Density, FFV, WAXD peak positions (2θ), and calculated *d*-spacing values of TPI-PHI and TPI-PBO films.

Polymer	Density (g cm^{-3})	FFV (%)	2θ (°)		*d*-spacing (Å)	
			A	B	A	B
TPI-PHI-0.25	1.490	15.6	12.3	16.0	7.2	5.5
TPI-PHI-0.50	1.451	16.0	12.3	15.9	7.2	5.6
TPI-PHI-0.75	1.407	16.6	12.1	15.9	7.3	5.6
TPI-PBO-0.25	1.409	20.4	11.8	14.8	7.5	6.0
TPI-PBO-0.50	1.381	20.0	11.8	14.6	7.5	6.1
TPI-PBO-0.75	1.361	19.3	11.6	14.6	7.6	6.1

consistent with the fact that triptycene units tend to increase the FFV of corresponding polymers by introducing large amount of internal free volume [50] as well as disrupting chain packing due to their bulkiness. However, an opposite trend was observed for the resulting TPI-PBO copolymers, i.e., the FFV decreases with the mole content of non-TR-able triptycene-containing 6FDA-TPDAm units. This observation implies that the imide-to-benzoxazole conversion has more significant impact on the FFV and microporosity than the incorporation of triptycene-containing polyimide segments. Therefore, the TPI-PBO-0.25 shows the highest increase (31%) in FFV after TR process as well as the largest FFV of 20.4% among all copolymers due to the highest mole fraction of PBO segments.

Polymer chain packing structures in the films were further examined by wide-angle X-ray diffraction (WAXD), and the results are shown in Table 1 and Fig. 4. Two broad haloes (i.e., A and B) are observed for both the precursors and the thermally treated films, implying primarily amorphous chain packing structures in all samples. The TPI-PHI precursor films exhibit diffraction peaks located at $2\theta = \sim 12.3^{\circ}$ and $\sim 16^{\circ}$, which correspond to *d*-spacing values of ~7.2 Å and 5.6 Å, respectively (Fig. 4). The *d*-spacing value of peak A (7.2 Å) is much higher than those of most of previously reported poly(benzoxazole-*co*-imide) precursors [12,51,52], and the value is very comparable to the molecule size of triptycene [50]; therefore, peak A can be assigned to the inter-chain distance of triptycene-containing TPI (6FDA-TPDAm) segments. Peak B with a smaller *d*-spacing value can be identified as the inter-chain distance of PHI (6FDA-6FAP) segments. The relative intensity of peak A and B increases with increasing mole fraction of TPI unit (Fig. 4a), which is reflected as increased FFV values (Table 1). The results further confirm that triptycene units can efficiently disrupt chain packing and introduce high FFV and microporosity in the films. Compared to copolyimide precursors, the *d*-spacing values of both peaks are higher in the thermally treated TPI-PBO copolymers, suggesting that the more rigid, coplanar benzoxazole structures prevent tight chain packing leading to even higher inter-chain distance and FFV. In particular, the relative increase in *d*-spacing value for peak B upon TR process is higher than that of peak A, implying more significant changes of chain conformation and packing structures during the thermal rearrangement.

Microcavity size and pore size distribution (PSD) of the TPI-PBO films were quantitatively analyzed by positron annihilation lifetime spectroscopy (PALS). One *o*-Ps component, i.e., τ_3, which has annihilation lifetime in the range of 1.9 − 2.8 ns, was observed in TPI-PBO films, implying unimodal pore size distribution of the TPI-PBO films. The average microcavity size was calculated according to Eq. (2) and the results are tabulated in Table 2. PALS analysis reveals that copolymers with higher PBO fractions, i.e., TPI-PBO-0.25 and TPI-PBO-0.5 films, displayed markedly higher average micropore size than TPI-PBO-0.75 with lower PBO content, suggesting that PBO structure is the dominating factor in determining the average microcavity size. The slightly higher average micropore size of TPI-PBO-0.5 compared to TPI-PBO-0.25 is likely due to its higher triptycene content. This seems to suggest that when the PBO component reached dominant content (e.g., ≥ 50%), the effect of triptycene moieties plays a more important role in contributing towards the microcavity size. Additionally, a clear increasing trend of *o*-positronium intensity, which indicates the concentration of cavities, is observed with increasing PBO mole fraction in TPI-PBO films. The results correlate well with the FFV data and *d*-spacing results from WAXD, confirming the significance of PBO structure in constructing microporous structures.

Different from the bimodal size distribution observed in the non-triptycene containing aPBO [14] and some high-free-volume polymers such as PTMSP and PIM-1 [53], the TPI-PBO films in this study display a unimodal pore size distribution with the microcavity diameter ranging from ~ 3 to 14 Å that covers both the ultra-microporous ($d < 7$ Å) and the microporous ($10 < d < 20$ Å) regions [5,6]. However, previous study has demonstrated that in some cases it can be difficult to define whether a unimodal or a bimodal fit is applicable during PSD analysis due to the nature of micropore architecture [54]. The PSD peak intensity increases as the PBO content increases, which is consistent with FFV and WAXD results, indicating TR process generated more microcavities. Notably, as evidenced by the full width at half maximum (FWHM) values in Fig. 5, the distribution of cavity sizes becomes narrower with the increase of PBO mole content in the TPI-PBO copolymers. This trend suggests that the changes in molecular configuration and chain conformation during TR process create well-connected diffusion pathways with narrow pore size distribution, which is ideal for efficient molecule separations based on size discrimination mechanism [9].

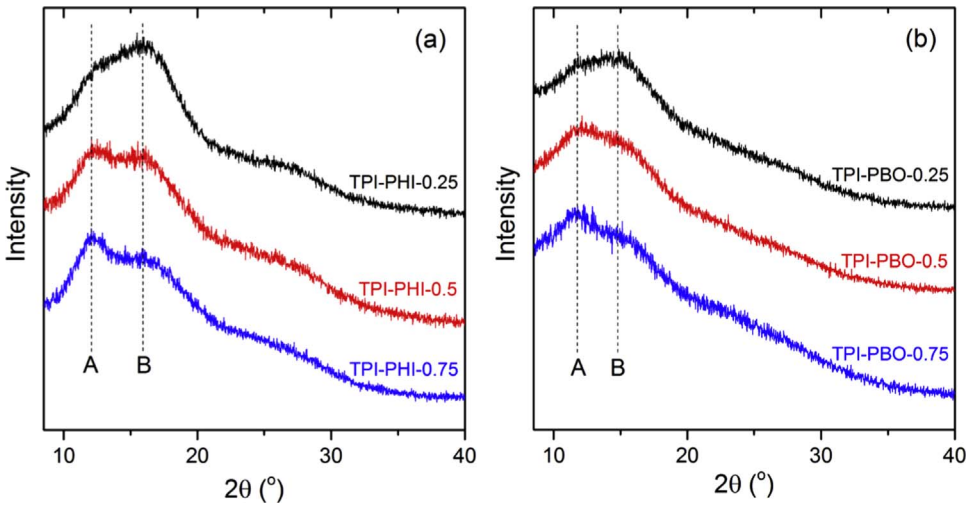

Fig. 4. WAXD patterns of (a) TPI-PHI copolyimide precursors and (b) TPI-PBO copolymers.

Table 2
Microcavity size characterization of TPI-PBO copolymer membranes measured by PALS.

polymer	τ_3 (ns)	I_3 (%)	cavity diameter d_3 (Å)	τ_4 (ns)	I_4 (%)	cavity diameter d_4 (Å)
TPI-PBO-0.25	2.70 ± 0.04	3.3 ± 0.0	6.85 ± 0.06	–	–	–
TPI-PBO-0.50	2.77 ± 0.07	2.9 ± 0.1	6.94 ± 0.09	–	–	–
TPI-PBO-0.75	1.93 ± 0.07	2.6 ± 0.1	5.58 ± 0.13	–	–	–
aPBO [14]	1.06 ± 0.09	7.1 ± 0.7	3.51 ± 0.28	3.90 ± 0.04	12.7 ± 0.7	8.37 ± 0.04
PTMSP [53]	1.7	7.4	5.1	8.8	34	12.4
PIM-1 [53]	2.06	6.15	5.8	6.28	18.6	10.6

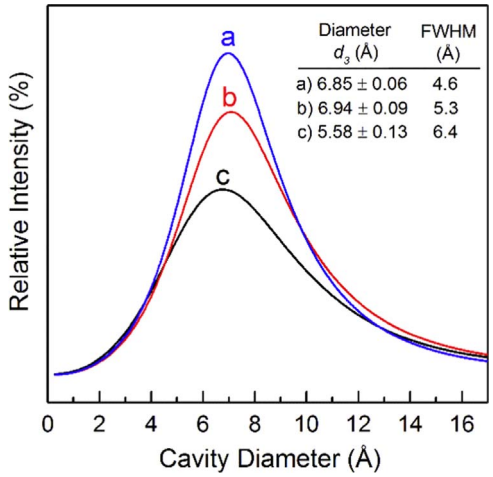

Fig. 5. Micropore size and size distribution of (a) TPI-PBO-0.25, (b) TPI-PBO-0.50, and (c) TPI-PBO-0.75 from PALS measurements. The average micropore diameter and full width at half maximum (FWHM) are listed in the inset table.

3.4. Mechanical properties

The mechanical strength is one of the critical parameters to advance practical implementation of TR membranes in industrial applications because sufficient mechanical strength is always required to not only withstand the high operating pressure but also enable membrane module fabrication and transportation. Mechanical properties in terms of elastic modulus, tensile strength and elongation at break for both TPI-PHI precursors and thermally converted TPI-PBO films were examined in uniaxial tension tests and the results are listed in Table 3 and pictures of the converted TPI-PBO films are shown in Fig. S3. The TPI-PHI precursor films display high mechanical strength with tensile strengths of 56 − 64 MPa, elongation at break of 2.8 − 3.2%, and initial modulus values of 2.62 − 2.88 GPa. After thermal treatment at 450 °C for 0.5 h, the TPI-PBO films exhibit lower mechanical strengths as compared with their corresponding precursor films (Table 3). For instance, both tensile strength and elongation at break of TPI-PBO-0.25 are around 70% lower than those of TPI-PHI-0.25, along with a ~10% decrease in the elastic modulus. The deterioration of mechanical strengths is frequently observed in TR polymers [35,55], and can be ascribed to the increased chain rigidity of PBO structure which causes fast deformation during tensile test, as well as possible thermal decomposition at high temperatures (Table S2).

Table 3
Mechanical properties of the PTI-PHI precursors and thermally rearranged TPI-PBO films.

Polymer	Elastic modulus (GPa)	Tensile strength (MPa)	Elongation at break (%)
TPI-PHI-0.25	2.82 ± 0.39	63 ± 8	3.2 ± 1.2
TPI-PHI-0.50	2.77 ± 0.11	64 ± 5	2.9 ± 0.3
TPI-PHI-0.75	2.62 ± 0.38	56 ± 6	2.8 ± 0.4
TPI-PBO-0.25	2.52 ± 0.75	16 ± 3	0.7 ± 0.1
TPI-PBO-0.50	2.27 ± 0.26	16 ± 3	0.7 ± 0.1
TPI-PBO-0.75	2.46 ± 0.40	13 ± 4	0.6 ± 0.2

Mechanical properties of TPI-PBO films were also compared with those of several previously reported PBO films with similar thermal treatment protocols (Table S3), and some important characteristics including the molecule weight of the precursors, thermal treatment protocol, and PBO conversion of these PBO films were also included for comparison. As shown, a spirobisindane-containing PBO film, i.e., spiroTR-PBO-BP, displayed much better tensile strength and elongation at break than those of TPI-PBO films in this study [21]. However, it should be mentioned that the molecule weight for spiroTR-PBO-BP precursor is about twice those of the TPI-PBO films in this study, which could be a dominating factor contributing to the excellent mechanical properties. A similar trend was also observed for HAB-6FDA-TR450 in Table S3 [55]. Recent studies showed that incorporating flexible ether linkages or methylene groups in poly(benzoxazole-*co*-imide) copolymers increased chain packing efficiency leading to enhanced mechanical strengths of the PBO-based copolymer membranes [12,22–24]. However, most of the mechanical properties in these studies were reported on the films thermally treated at 400 °C, which was always accompanied by incomplete TR conversion compromising their transport properties. Moreover, it should be mentioned that mechanical properties of PBO homopolymers prepared under similar condition (450 °C) have been sparsely reported, most likely due to their poor mechanical strength in that the films were too brittle for tensile testing, as shown in Table S3 [55]. Considering all factors discussed above, the incorporation of non-TR-able triptycene-containing polyimide segments in this study resulted in the improvement of mechanical properties of TPI-PBO films. Additionally, the incorporation of triptycene may induce π-π stacking attraction between benzene rings [32], which may also contribute to the improved mechanical strength of the TPI-PBO films. On the other hand, mechanical properties of TPI-PBO copolymers do not show a defined trend as a function of PBO content. This is again because other factors such as molecular weight may also influence the mechanical properties. For example, TPI-PBO-0.75 exhibited the lowest mechanical strength, possibly due to the relatively low molecular weight compared to the other polymers (Table S1).

3.5. Gas transport properties

Pure gas permeation experiments were conducted with five ultra-high-purity gases, i.e., H_2, CH_4, N_2, O_2, and CO_2, to study the gas transport properties of the triptycene-containing poly(benzoxazole-*co*-imide) films as well as to examine how the copolymer composition and structure affect the gas transport properties. Pure gas permeability, ideal selectivity, diffusivity coefficient, and solubility coefficient of the films are summarized in Table 4. Representative PBO and PBO-*co*-PI films are also included for comparison. Generally, the permeability coefficients (P) of the TPI-PBO films follow the reverse gas kinetic diameter order, i.e., $P(H_2) > P(CO_2) > P(O_2) > P(N_2) > P(CH_4)$, indicating that gas transport in the films is dominated by kinetic diffusion. Diffusivity coefficient (D) results reflect the similar order of gas kinetic diameter, while the deviation of CO_2 diffusivity coefficient can be ascribed to the favorable interaction between the polarizable CO_2 molecules and imide-*co*-benzoxazole structures through dipole-quadrupole interaction, as evidenced by the highest CO_2 solubility

Table 4
Single gas permeabilities (*P*), ideal selectivities (α), diffusivity coefficients (*D*), and solubility coefficient (*S*) for triptycene-containing TPI-PBO films (3 atm, 35 °C).

Polymer		Permeability (barrer)					Ideal selectivity (α)			
		H_2	CO_2	O_2	N_2	CH_4	H_2/N_2	H_2/CH_4	CO_2/CH_4	O_2/N_2
TPI-PBO-0.25										
[a]*P*		878	952	197	53	34	17	26	28	3.7
[b]*D*		–	481	1042	247	48	–	–	10	4.2
S		–	15	1.4	1.6	5.4	–	–	2.8	0.88
TPI-PBO-0.50										
P		762	667	141	34	25	22	30	27	4.2
D		–	304	753	194	31	–	–	9.9	3.9
S		–	17	1.4	1.3	6.2	–	–	2.7	1.1
TPI-PBO-0.75										
P		574	505	107	25	18	23	32	28	4.3
D		–	216	476	122	25	–	–	8.8	3.9
S		–	18	1.7	1.6	5.6	–	–	3.2	1.1
aPBO [14]	*P*	408	398	81	19	12	22	34	33	4.3
APAF5-DAM5 [24]	*P*	287	270	53	13	8.3	23	35	32	4.2
R-TR-PBOIa-2h [12]	*P*	191	114	25	5.0	2.7	38	71	42	5.0
AD-cPBO-PI [59]	*P*	663	638	167	53	48.1	13	14	13	3.2
PIM-1 [60]	*P*	3600	6500	1300	340	430	11	8.4	15	3.8
PIM-EA-TB [7]	*P*	8114	7696	2294	580	774	14	10	9.9	4.0
PIM-Trip-TB [8]	*P*	8039	9709	2718	629	905	13	8.9	11	4.3
Matrimid® [61]	*P*	18	10	2.1	0.32	0.28	56	64	36	6.6

[a] Units: *P*, Barrer, 10^{-10} cm^3(STP)/cm·s·cmHg; *D*, 10^{-9} cm^2/s; *S*, cm^3(STP)/cm^3 atm.
[b] The diffusivity and solubility coefficients for H_2 were not shown due to its very short lag time.

coefficients among all gases (Table 4). The second highest CH_4 solubility coefficient may be attributed to the H-π interaction between CH_4 and triptycene moieties [56]. The permeabilities of the TPI-PBO films strongly depend on the chemical structures and PBO content of the copolymer films. As expected, the triptycene-containing TPI-PBO films exhibit higher gas permeabilities compared with some of the most permeable polyimides such as 6FDA-durene and 6FDA-DAM [57,58], as well as triptycene-based polyimides [28,29,38,47]. Specifically, gas permeabilities increase with the increasing PBO molar content in the copolymers, which implies that PBO segments play a more significant role in providing high gas permeabilities. For instance, the CO_2 permeability increased by 88% from 505 to 952 Barrer when the PBO mole fraction increased from 25% in TPI-PBO-0.25 film to 75% in TPI-PBO-0.75 film. The significant increase of gas permeabilities with increasing mole fraction of PBO units is primarily due to the dramatic increase in gas diffusivity coefficients, as these copolymers have almost the same solubility coefficients (Table 4). The results are consistent with FFV and PALS results, confirming that the formation of rigid PBO structure results in enlarged microcavity size.

The incorporation of triptycene in this study is expected to address the low gas permeabilities of current poly(benzoxazole-*co*-imide) due to tight chain packing of relatively flexible polyimide segments [12,23,24,59,62,63]. As shown in Table 4, this has been evidenced by the higher gas permeabilities of TPI-PBOs than those of non-triptycene-containing PBOs and PI-*co*-PBO copolymers. For example, all TPI-PBO films display higher gas permeabilities than those of aPBO [14], which was fabricated from 6FDA-6FAP poly(hydroxyimide) precursor following a similar thermal treatment procedure. Specifically, the CO_2 permeability of TPI-PBO-0.75, which has the lowest PBO content (highest triptycene content of 75%), is 27% higher than that of aPBO [14], suggesting triptycene moieties can significantly improve gas permeabilities by disrupting chain packing. Additionally, TPI-PBO films also exhibit much higher gas permeabilities than those of recently reported poly(benzoxazole-co-imide)s, such as TR-PBOIs [24], R/B-TR-PBOIa/b (random/block poly(benzoxazole-*co*-imide)s) [12], TR-PBO-co-I [23], AD/HD-a/cPBO-PI (poly(benzoxazole-co-imide)s prepared from different monomer combinations and imidization methods) [59], and PIa-d (poly(benzoxazole-*co*-imide)s with isomerism) [63]. It should be mentioned that gas transport properties also sensitively depend on the thermal treatment protocol and especially on PBO conversion degree. Therefore, the thermal treatment protocol, PBO conversion ratio and gas transport properties of recently reported TR-PBOIs were summarized in Table S4, which were compared with those of TPI-PBO films in this study. For instance, the CO_2 permeability of TPI-PBO-0.25 film in this study is ~15 times that of APAF8-ODA2 although both copolymers share almost the same PBO molar content, the same PBO conversion ratio of 100%, and similar chemical structure except that triptycene replaced ODA as the non-TR-able polyimide units [24]. Notably, the significant increase in gas permeabilities of TPI-PBO films is accompanied with good gas selectivities comparable to other poly (benzoxazole-*co*-imide) films.

The overall gas separation performance of triptycene-containing TPI-PBO copolymers are further summarized in the Robeson upper bound plots of permeability-selectivity trade-off for H_2/CH_4, H_2/N_2, and CO_2/CH_4 gas pairs, along with commercial Matrimid® polyimide and previously reported poly(benzoxazole-*co*-imide) films for comparison. As shown in Fig. 6, all triptycene-containing TPI-PBO films are about two orders of magnitude more permeable than the benchmark Matrimid® polyimide for all relevant gas separations. Moreover, the TPI-PBO films are much more permeable than many previously reported poly(benzoxazole-*co*-imide) films including TR-PBOIs [24], R/B-TR-PBOIa/b [12], TR-PBO-co-I [23], AD/HD-a/cPBO-PI [59], and PIa-d [63], with slightly lower gas selectivities (Table 4 and Fig. 6). When compared to some of the most permeable polymeric membranes such as PIM-1 [60] and Tröger's based polymers [7,8], TPI-PBO films exhibit much higher selectivities along with high permeabilities. Several triptycene-containing TPI-PBO films outperform the 2008 Robeson upper bound for H_2/CH_4 separation and exceed or approach the 2008 upper bounds for H_2/N_2 and CO_2/CH_4 separation. The permeability-selectivity results suggest that the incorporation of triptycene units in poly(benzoxazole-*co*-imide)s helps to optimize the microcavity architecture leading to superior performance highly desirable for hydrogen separation and natural gas purification.

4. Conclusions

A series of triptycene-containing poly(benzoxazole-*co*-imide) TR copolymers (TPI-PBO) with excellent gas separation performance were fabricated by thermal rearrangement of triptycene-containing poly (imide-*co*-hydroxyimide) precursors. Due to the incorporation of non-

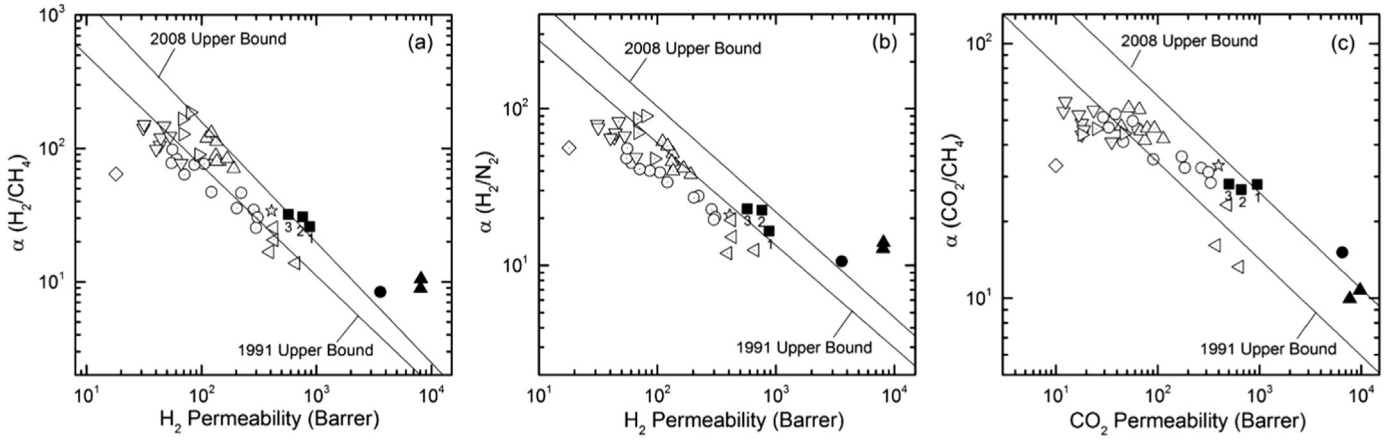

Fig. 6. Permeability-selectivity upper bound plots of TPI-PBO-0.25 (■, 1), TPI-PBO-0.50 (■, 2), and TPI-PBO-0.75 (■, 3) for (a) H_2/CH_4, (b) H_2/N_2 and (c) CO_2/CH_4 gas pairs. Other benchmark polymers are included for comparison: aPBO (☆) [14], Matrimid® (◇) [61], TR-PBOIs (○) [24], R/B-TR-PBOIa/b (△) [12], TR-PBO-*co*-I (▽) [23], AD/HD-a/cPBO-PI (◁) [59], PIa-d (▷) [63], PIM-1 (•) [60], and PIM-Tröger's base (▲) [7,8].

TR-able polyimide segments, the resulting TPI-PBO films exhibited good mechanical properties. The fractional free volume and *d*-spacing values of the thermally converted films increased dramatically upon TR process as compared to their corresponding precursors, and the FFV of copolymer films increased with the PBO molar fraction in the copolymers. All triptycene-containing poly(benzoxazole-*co*-imide) films in this study exhibited unimodal pore size distribution with microcavity diameter spanning from ~ 3–14 Å covering both the ultra-microporous ($d < 7$ Å) and the microporous ($10 < d < 20$ Å) regions. The averaged microcavity size generally increased with increasing PBO content in the copolymers. Significant improvements in gas permeabilities were achieved in these triptycene-containing TPI-PBO copolymers when compared to previously reported poly(benzoxazole-*co*-imide)s, due to the disruption of chain packing by the bulky and rigid triptycene units. Specifically, the triptycene-containing poly(benzoxazole-*co*-imide) films displayed excellent gas separation performance for H_2/CH_4, H_2/N_2, and CO_2/CH_4 gas pairs exceeding or approaching the 2008 upper bounds.

Acknowledgements

R. Guo gratefully acknowledges the financial support of the Division of Chemical Sciences, Biosciences, and Geosciences, Office of Basic Energy Sciences of the U.S. Department of Energy (DOE) under Award DE-SC0010330. C. M. Doherty acknowledges the support of Australian Research Council under award DE140101359. We thank Prof. Haifeng Gao at University of Notre Dame for the use of GPC.

Appendix A. Supporting information

Supplementary data associated with this article can be found in the online version at http://dx.doi.org/10.1016/j.memsci.2018.01.052.

References

[1] R.W. Baker, B.T. Low, Gas separation membrane materials: a perspective, Macromolecules 47 (2014) 6999–7013.
[2] Y. Yampolskii, Polymeric gas separation membranes, Macromolecules 45 (2012) 3298–3311.
[3] D.F. Sanders, Z.P. Smith, R. Guo, L.M. Robeson, J.E. McGrath, D.R. Paul, B.D. Freeman, Energy-efficient polymeric gas separation membranes for a sustainable future: a review, Polymer 54 (2013) 4729–4761.
[4] P.M. Budd, E.S. Elabas, B.S. Ghanem, S. Makhseed, N.B. McKeown, K.J. Msayib, C.E. Tattershall, D. Wang, Solution-processed, organophilic membrane derived from a polymer of intrinsic microporosity, Adv. Mater. 16 (2004) 456–459.
[5] B.S. Ghanem, R. Swaidan, X. Ma, E. Litwiller, I. Pinnau, Energy-efficient hydrogen separation by AB-type ladder-polymer molecular sieves, Adv. Mater. 26 (2014) 6696–6700.
[6] B.S. Ghanem, R. Swaidan, E. Litwiller, I. Pinnau, Ultra-microporous triptycene-based polyimide membranes for high-performance gas separation, Adv. Mater. 26 (2014) 3688–3692.
[7] M. Carta, R. Malpass-Evans, M. Croad, Y. Rogan, J.C. Jansen, P. Bernardo, F. Bazzarelli, N.B. McKeown, An efficient polymer molecular sieve for membrane gas separations, Science 339 (2013) 303–307.
[8] M. Carta, M. Croad, R. Malpass-Evans, J.C. Jansen, P. Bernardo, G. Clarizia, K. Friess, M. Lanc, N.B. McKeown, Triptycene induced enhancement of membrane gas selectivity for microporous Troger's base polymers, Adv. Mater. 26 (2014) 3526–3531.
[9] H.B. Park, C.H. Jung, Y.M. Lee, A.J. Hill, S.J. Pas, S.T. Mudie, E. Van Wagner, B.D. Freeman, D.J. Cookson, Polymers with cavities tuned for fast selective transport of small molecules and ions, Science 318 (2007) 254–258.
[10] L.M. Robeson, Correlation of separation factor versus permeability for polymeric membranes, J. Membr. Sci. 62 (1991) 165–185.
[11] L.M. Robeson, The upper bound revisited, J. Membr. Sci. 320 (2008) 390–400.
[12] Y. Zhuang, J.G. Seong, W.H. Lee, Y.S. Do, M.J. Lee, G. Wang, M.D. Guiver, Y.M. Lee, Mechanically tough, thermally rearranged (tr) random/block poly(benzoxazole-co-imide) gas separation membranes, Macromolecules 48 (2015) 5286–5299.
[13] Y. Jiang, F.T. Willmore, D. Sanders, Z.P. Smith, C.P. Ribeiro, C.M. Doherty, A. Thornton, A.J. Hill, B.D. Freeman, I.C. Sanchez, Cavity size, sorption and transport characteristics of thermally rearranged (TR) polymers, Polymer 52 (2011) 2244–2254.
[14] S.H. Han, N. Misdan, S. Kim, C.M. Doherty, A.J. Hill, Y.M. Lee, Thermally rearranged (TR) polybenzoxazole: effects of diverse imidization routes on physical properties and gas transport behaviors, Macromolecules 43 (2010) 7657–7667.
[15] R. Guo, D.F. Sanders, Z.P. Smith, B.D. Freeman, D.R. Paul, J.E. McGrath, Synthesis and characterization of thermally rearranged (TR) polymers: influence of *ortho*-positioned functional groups of polyimide precursors on TR process and gas transport properties, J. Mater. Chem. A 1 (2013) 262–272.
[16] R. Guo, D.F. Sanders, Z.P. Smith, B.D. Freeman, D.R. Paul, J.E. McGrath, Synthesis and characterization of thermally rearranged (TR) polymers: effect of glass transition temperature of aromatic poly(hydroxyimide) precursors on TR process and gas permeation properties, J. Mater. Chem. A 1 (2013) 6063–6072.
[17] H. Wang, T.-S. Chung, The evolution of physicochemical and gas transport properties of thermally rearranged polyhydroxyamide (PHA), J. Membr. Sci. 385 (2011) 86–95.
[18] S.H. Han, H.J. Kwon, K.Y. Kim, J.G. Seong, C.H. Park, S. Kim, C.M. Doherty, A.W. Thornton, A.J. Hill, A.E. Lozano, K.A. Berchtoldf, Y.M. Lee, Tuning microcavities in thermally rearranged polymer membranes for CO_2 capture, Phys. Chem. Chem. Phys. 14 (2012) 4365–4373.
[19] Z.P. Smith, K. Czenkusch, S. Wi, K.L. Gleason, G. Hernandez, C.M. Doherty, K. Konstas, T.J. Bastow, C. Alvarez, A.J. Hill, A.E. Lozano, D.R. Paul, B.D. Freeman, Investigation of the chemical and morphological structure of thermally rearranged polymers, Polymer 55 (2014) 6649–6657.
[20] A. Kushwaha, M.E. Dose, Z.P. Smith, S. Luo, B.D. Freeman, R. Guo, Preparation and properties of polybenzoxazole-based gas separation membranes: a comparative study between thermal rearrangement (TR) of poly(hydroxyimide) and thermal cyclodehydration of poly(hydroxyamide), Polymer 78 (2015) 81–93.
[21] S. Li, H.J. Jo, S.H. Han, C.H. Park, S. Kim, P.M. Budd, Y.M. Lee, Mechanically robust thermally rearranged (TR) polymer membranes with spirobisindane for gas separation, J. Membr. Sci. 434 (2013) 137–147.
[22] M. Calle, Y.M. Lee, Thermally rearranged (TR) poly(ether-benzoxazole) membranes for gas separation, Macromolecules 44 (2011) 1156–1165.
[23] C.Y. Soo, H.J. Jo, Y.M. Lee, J.R. Quay, M.K. Murphy, Effect of the chemical structure of various diamines on the gas separation of thermally rearranged poly(benzoxazole-co-imide) (TR-PBO-co-I) membranes, J. Membr. Sci. 444 (2013) 365–377.
[24] H.J. Jo, C.Y. Soo, G. Dong, Y.S. Do, H.H. Wang, M.J. Lee, J.R. Quay, M.K. Murphy, Y.M. Lee, Thermally rearranged poly(benzoxazole-co-imide) membranes with superior mechanical strength for gas separation obtained by tuning chain rigidity,

Macromolecules 48 (2015) 2194–2202.
[25] Y.M. Xu, N.L. Le, J. Zuo, T.S. Chung, Aromatic polyimide and crosslinked thermally rearranged poly (benzoxazole-co-imide) membranes for isopropanol dehydration via pervaporation, J. Membr. Sci. 499 (2016) 317–325.
[26] Y.J. Cho, H.B. Park, High performance polyimide with high internal free volume elements, Macromol. Rapid Commun. 32 (2011) 579–586.
[27] J.R. Weidman, R. Guo, The use of iptycenes in rational macromolecular design for gas separation membrane applications, Ind. Eng. Chem. Res. 56 (2017) 4220–4236.
[28] N. Alaslai, B. Ghanem, F. Alghunaimi, I. Pinnau, High-performance intrinsically microporous dihydroxyl-functionalized triptycene-based polyimide for natural gas separation, Polymer 91 (2016) 128–135.
[29] J.R. Wiegand, Z.P. Smith, Q. Liu, C.T. Patterson, B.D. Freeman, R. Guo, Synthesis and characterization of triptycene-based polyimides with tunable high fractional free volume for gas separation membranes, J. Mater. Chem. A 2 (2014) 13309–13320.
[30] S. Luo, Q. Liu, B. Zhang, J.R. Wiegand, B.D. Freeman, R. Guo, Pentiptycene-based polyimides with hierarchically controlled molecular cavity architecture for efficient membrane gas separation, J. Membr. Sci. 480 (2015) 20–30.
[31] S. Luo, K.A. Stevens, J.S. Park, J.D. Moon, Q. Liu, B.D. Freeman, R. Guo, Highly CO_2-selective gas separation membranes based on segmented copolymers of poly (ethylene oxide) reinforced with pentiptycene-containing polyimide hard segments, ACS Appl. Mater. Interfaces 8 (2016) 2306–2317.
[32] S. Luo, J.R. Wiegand, P. Gao, C.M. Doherty, A.J. Hill, R. Guo, Molecular origins of fast and selective gas transport in pentiptycene-containing polyimide membranes and their physical aging behavior, J. Membr. Sci. 518 (2016) 100–109.
[33] S. Luo, J.R. Wiegand, B. Kazanowska, C.M. Doherty, K. Konstas, A.J. Hill, R. Guo, Finely tuning the free volume architecture in iptycene-containing polyimides for highly selective and fast hydrogen transport, Macromolecules 49 (2016) 3395–3405.
[34] S. Kim, Y.M. Lee, Rigid and microporous polymers for gas separation membranes, Prog. Polym. Sci. 43 (2015) 1–32.
[35] S.J. Luo, J.Y. Liu, H.Q. Lin, B.A. Kazanowska, M.D. Hunckler, R.K. Roeder, R.L. Guo, Preparation and gas transport properties of triptycene-containing polybenzoxazole (PBO)-based polymers derived from thermal rearrangement (TR) and thermal cyclodehydration (TC) processes, J. Mater. Chem. A 4 (2016) 17050–17062.
[36] F. Alghunaimi, B. Ghanem, Y.G. Wang, O. Salinas, N. Alaslai, I. Pinnau, Synthesis and gas permeation properties of a novel thermally-rearranged polybenzoxazole made from an intrinsically microporous hydroxyl-functionalized triptycene-based polyimide precursor, Polymer 121 (2017) 9–16.
[37] P.D. Bartlett, M.J. Ryan, S.G. Cohen, Triptycene (9,10-*o*-benzenoanthracene), J. Am. Chem. Soc. 64 (1942) 2649–2653.
[38] J.R. Weidman, S. Luo, J.M. Breier, P. Buckley, P. Gao, R. Guo, Triptycene-based copolyimides with tailored backbone rigidity for enhanced gas transport, Polymer 126 (2017) 314–323.
[39] ASTM D882-12, Standard Test Method for Tensile Properties of Thin Plastic Sheeting, ASTM International, West Conshohocken, PA, in, 2012.
[40] A. Bondi, van der Waals volumes and radii, J. Phys. Chem. A 68 (1964) 441–451.
[41] J.Y. Park, D.R. Paul, Correlation and prediction of gas permeability in glassy polymer membrane materials via a modified free volume based group contribution method, J. Membr. Sci. 125 (1997) 23–39.
[42] Y. Yampolskii, V. Shantarovich, Materials Science of Membranes for Gas and Vapor Separation, John Wiley & Sons Ltd., Chichester, 2006.
[43] S.J. Tao, Positronium annihilation in molecular substances, J. Chem. Phys. 56 (1972) 5499–5510.
[44] M. Eldrup, D. Lightbody, J.N. Sherwood, The temperature-dependence of positron lifetimes in solid pivalic acid, Chem. Phys. 63 (1981) 51–58.
[45] C. Pascual-Izarra, A.W. Dong, S.J. Pas, A.J. Hill, B.J. Boyd, C.J. Drummond, Advanced fitting algorithms for analysing positron annihilation lifetime spectra, J. Nucl. Instrum. Methods A 603 (2009) 456–466.
[46] H. Lin, B.D. Freeman, Permeation and diffusion, in: H. Czichos, T. Saito, L. Smith (Eds.), Springer Handbook of Material Measurement Methods, Springer, New York, 2006, pp. 371–387.
[47] J.R. Weidman, S.J. Luo, Q.N. Zhang, R.L. Guo, Structure manipulation in triptycene-based polyimides through main chain geometry variation and its effect on gas transport properties, Ind. Eng. Chem. Res. 56 (2017) 1868–1879.
[48] M. Calle, Y. Chan, H.J. Jo, Y.M. Lee, The relationship between the chemical structure and thermal conversion temperatures of thermally rearranged (TR) polymers, Polymer 53 (2012) 2783–2791.
[49] H.B. Park, S.H. Han, C.H. Jung, Y.M. Lee, A.J. Hill, Thermally rearranged (TR) polymer membranes for CO_2 separation, J. Membr. Sci. 359 (2010) 11–24.
[50] N.T. Tsui, A.J. Paraskos, L. Torun, T.M. Swager, E.L. Thomas, Minimization of internal molecular free volume: a mechanism for the simultaneous enhancement of polymer stiffness, strength, and ductility, Macromolecules 39 (2006) 3350–3358.
[51] M. Calle, H.J. Jo, C.M. Doherty, A.J. Hill, Y.M. Lee, Cross-linked thermally rearranged poly(benzoxazole-co-imide) membranes prepared from ortho-hydroxycopolyimides containing pendant carboxyl groups and gas separation properties, Macromolecules 48 (2015) 2603–2613.
[52] M. Calle, C.M. Doherty, A.J. Hill, Y.M. Lee, Cross-linked thermally rearranged poly (benzoxazole-co-imide) membranes for gas separation, Macromolecules 46 (2013) 8179–8189.
[53] C.L. Staiger, S.J. Pas, A.J. Hill, C.J. Cornelius, Gas separation, free volume distribution, and physical aging of a highly microporous spirobisindane polymer, Chem. Mater. 20 (2008) 2606–2608.
[54] Y.Y. Jiang, F.T. Willmore, D. Sanders, Z.P. Smith, C.P. Ribeiro, C.M. Doherty, A. Thornton, A.J. Hill, B.D. Freeman, I.C. Sanchez, Cavity size, sorption and transport characteristics of thermally rearranged (TR) polymers, Polymer 52 (2011) 2244–2254.
[55] Q. Liu, D.R. Paul, B.D. Freeman, Gas permeation and mechanical properties of thermally rearranged (TR) copolyimides, Polymer 82 (2016) 378–391.
[56] P. Mohanty, L.D. Kull, K. Landskron, Porous covalent electron-rich organonitridic frameworks as highly selective sorbents for methane and carbon dioxide, Nat. Commun. 2 (2011) 401.
[57] K. Tanaka, M. Okano, H. Toshino, H. Kita, K.I. Okamoto, Effect of methyl substituents on permeability and permselectivity of gases in polyimides prepared from methyl-substituted phenylenediamines, J. Polym. Sci. Part B: Polym. Phys. 30 (1992) 907–914.
[58] S. Japip, H. Wang, Y.C. Xiao, T.S. Chung, Highly permeable zeolitic imidazolate framework (ZIF)−71 nano-particles enhanced polyimide membranes for gas separation, J. Membr. Sci. 467 (2014) 162–174.
[59] S. Kim, K.T. Woo, J.M. Lee, J.R. Quay, M.K. Murphy, Y.M. Lee, Gas sorption, diffusion, and permeation in thermally rearranged poly(benzoxazole-co-imide) membranes, J. Membr. Sci. 453 (2014) 556–565.
[60] S. Thomas, I. Pinnau, N. Du, M.D. Guiver, Pure- and mixed-gas permeation properties of a microporous spirobisindane-based ladder polymer (PIM-1), J. Membr. Sci. 333 (2009) 125–131.
[61] Y. Zhang, I.H. Musseman, J.P. Ferraris, K.J. Balkus Jr., Gas permeability properties of Matrimid® membranes containing the metal-organic framework Cu-BPY-HFS, J. Membr. Sci. 313 (2008) 170–181.
[62] C.A. Scholes, C.P. Ribeiro, S.E. Kentish, B.D. Freeman, Thermal rearranged poly (benzoxazole-co-imide) membranes for CO_2 separation, J. Membr. Sci. 450 (2014) 72–80.
[63] Y.B. Zhuang, J.G. Seong, Y.S. Do, H.J. Jo, M.J. Lee, G. Wang, M.D. Guiver, Y.M. Lee, Effect of isomerism on molecular packing and gas transport properties of poly (benzoxazole-co-imide)s, Macromolecules 47 (2014) 7947–7957.